Int. J. Electrochem. Sci., 17 **(2022)** Article Number: 22015, doi: 10.20964/2022.01.27

International Journal of
ELECTROCHEMICAL
SCIENCE
www.electrochemsci.org

Radio Frequency-Based Implantable Glucose Biosensor

Jin Tan[1,2], *Yao-Chuan Chang*[3], *Qing Tang*[1,2], *Yang-Li Yang*[4], *Ta-Feng Tseng*[1,2,*]

[1] School of Environmental and Chemical Engineering, Zhaoqing University, Guangdong Zhaoqing 526061, China
[2] Guangdong Provincial Key Laboratory of Environmental Health and Land Resource, Zhaoqing University, Guangdong Zhaoqing 526061, China
[3] School of Physical Education and Health, Zhaoqing University, Guangdong Zhaoqing 526061, China
[4] Department of Biomedical Engineering, Chung-Yuan Christian University, Chung Li 32023, Taiwan
[*]E-mail: joseph.vnp@gmail.com

Received: 25 August 2021 / *Accepted:* 1 November 2021 / *Published:* 6 December 2021

Current implantable sensors are invasive, form fibrotic capsules, and are susceptible to a disconnection between the sensor and the controller. Here, we have developed an implantable wireless glucose monitoring system. This device is composed of an external controller to serve as a human-system interface and an implantable sensor to electrochemically measure glucose levels. Communication between the controller and the sensor is through a pair of an antenna (or coils) using peer-to-peer radio frequency (RF) technology. In addition, the implant's power is supplied by the controller through RF coupling. Wireless RF technology allows the controller to issue commands to the implant while receiving signals from the sensor. For implantation into rats, the entire implant unit was sealed with polydimethylsiloxane. The working electrodes were modified with various thermoplastic polyurethane (TPU) concentrations for glucose oxidase (GOx) immobilization and evaluated for protein adsorption in a simulated interstitial fluid environment by AUTOLAB. Results indicated that 30 mg/mL of TPU reduced protein adsorption most effectively. To evaluate the signal detection resolution, the device measured hydrogen peroxide levels and compared the data with AUTOLAB. Results indicate that the resolutions of our developed system and AUTOLAB were 114 and < 9.7 nA, respectively. The glucose biosensor with the TPU membrane was subsequently implanted in normoglycemic and hyperglycemic rats. The signal responses obtained from the study rats' ISF exhibited a significant difference when the blood glucose level changed. A comparison of intravenous and ISF glucose levels revealed a 30 to 170 minutes delay.

Keyword: Implantable; Glucose biosensor; Radio frequency; Class E power amplifier

1. INTRODUCTION

Diabetes mellitus is a heterogeneous metabolic condition characterized by hyperglycemia and sometimes results in renal, cardiovascular, or neurological tissue damage. One effective method for

treating diabetes mellitus is to continuously monitor and control blood sugar levels to avoid the aforementioned complications. Such as electrochemical [1, 2] and optical [3, 4]. Especially in electrochemical sensing technology, under the detection mechanism supported by enzyme and easy-to-use sensing technology, it has shown great commercial prospects for a long time. At present, some researchers use radio frequency (RF) for enzyme-free glucose detection, focusing on real-time accurate and fast reading, introducing S parameters, and fast measuring the target solution [5].

Regulation, however, often require diabetic patients to collect blood via finger pricking. This method is not only painful but only provides instantaneous data. As a result, two to three finger pricks are required to capture significant changes in blood glucose [6, 7]. Many researchers have reported using a closed-loop insulin system or artificial pancreas to regulate blood sugar levels; these consist of a glucose sensor and an insulin delivery pump to continuously monitor and minimize fluctuations in blood sugar levels. In particular, the glucose sensor is implantable, allowing communication with the artificial pancreas to maintain adequate blood sugar levels [8-12].

An issue associated with current systems, however, is that communication between the sensor implant and the monitoring user interface is faulty. Many current devices use invasive wire sensors in which the sensing element is implanted subcutaneously while the remainder of the wires is left outside of the skin for exterior access [13-15]. The implantation method and placement is thus an important consideration. For example, the sensor wires embedded into the subcutaneous tissue creates a new interface between the skin and wires. The interface is easily infected by bacteria such as bacillosis if there is no clean administration constantly applied. In addition, to minimize the area of the interface, the diameters of the sensor wires are demanded to be small. As time goes along, the wires can break apart. Consequently, it is imperative to address the potential communication failure between the two modules: the sensor implant and the outside monitor. Here, we developed a telemetry-capable implantable glucose sensor incorporated with a wireless communication module to solve this issue. The module is radio frequency based and consists of two major components: (1) an external subsystem responsible for transmitting power, issuing commands and receiving signals from (2) an internal subsystem serving glucose level readout and transmitting the readout to the external. The major component used in the wireless communication module is a Class E amplifier, which is an electrical current driving power switch generating a predefined resonant frequency electromagnetic wave through a coil. This wave is commonly termed radio frequency (RF), which can transmit in air and mediums. The reason we used the Class E technique is according to the following reports. Sokal et al. utilized a Class E amplifier to investigate the impact of switching frequency and transfer efficiency. The Class E transfer efficiency is near to 100 %, making it the best option for implantable device applications [16-20]. Furthermore, Class E switches can be used to make various current amplitudes and timing intervals to modulate and demodulate to form predefined communication sets of signals or commands between the external and internal subsystems. In 1992, Troyk et al. developed a closed-loop Class-E amplifier that successfully demonstrates that an implant unit can transmit data and power in subcutaneous tissues [21].

Another important consideration for the implantable device is the properties of its permeable membrane. Many researchers observe a decreased sensitivity of implantable biosensors resulting from the biofouling or absorption of biomolecules onto the sensor membrane [22-25]. Non-specific protein adsorption may instigate a foreign body reaction, which may lead to the formation of a fibrous capsule

[26-31] and create a diffusion barrier for the implanted biosensors. Consequently, the goal of our device is to prevent protein adsorption and diminish biofouling formation. The approach is to miniaturize the sensing components such as the working, reference, and counter (auxiliary) electrodes and perform in vitro tests using a simulated fluid containing the same protein concentration as interstitial fluids. In this study, we diluted human serum to form the interstitial fluid (ISF) surrogate for evaluating the performance of our implantable biosensor.

Polyurethane (PU) is a material commonly used for biomedical applications including vascular catheters, artificial organs, tissue replacement, and augmentations. In particular, thermoplastic polyurethane (TPU) is among the most important plastics for implantable devices because it demonstrates high tensile strength, toughness, degradation resistance, and biocompatibility. Additionally, TPU can immobilize enzymes for long-term use. Researchers typically use Tecoflex® EG-series TPU, similar to EG-80A, EG-85A, corresponding to the permeable membrane or immobilized enzyme [32-35]. In this paper, we used Tecoflex® EG-85A to study how different TPU concentrations can impact biosensor performance in an ISF surrogate test.

Our current work involves the fabrication of a bi-directional wireless transmission electrochemical biosensor consisting of an external control/monitoring subsystem and an internal implantable biosensor. The biosensor is tested by implanting into the subcutaneous tissue of the diabetic rat to continuously monitor glucose levels.

2. MATERIALS and METHODS

2.1. Fabrication of Radio Frequency-based Implantable Biosensor

The radio-frequency-based implantable biosensor consists of an external subsystem and an internal subsystem. The functional blocks of the external subsystem are shown in Figure 1(C) MSP430F149 (Dallas, Texas, U.S.A.) is used as the microprocessor for the external system. The unit possesses features including generating digital commands, processing data for real-time display on an LCD, and plotting through an RS232 port connected with a personal computer.

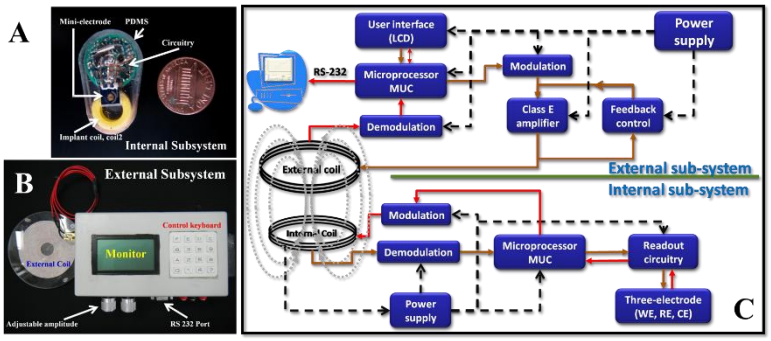

Figure 1. An overall implantable glucose monitoring system shows the flow of the major modules and the pictures of external and internal subsystems. (C) Functional block diagram of implantable glucose monitoring system. It is comprised of an (A) internal subsystem and an (B) external subsystem.

The commands are coded via a modulation circuit which translates the underlined signals into a carrying frequency of 820 kHz. Through the modulated signal, the internal subsystem receives commands to detect glucose. The data from the sensor is simultaneously coupled to the external system and presents a current response corresponding to the glucose concentration. The external antenna receives data from the internal unit which translates the data through the demodulation module. The external subsystem, shown in Figure 1-B, is composed of the external coil, the control keyboard, the RS 232 port, and the LCD monitor.

Figure 1(C) indicates the functional blocks of the internal subsystem, including a power manager, modulation/demodulation, electrochemical analyzer, microprocessor. To ensure its functionality, this implant unit was assembled with circuitry modules similar to those designed in the external unit. An internal coil couple the RF signals from the external coil. The coupled signal is processed concurrently, converted to direct current, and decoded into command signals. Electricity is supplied to all the circuits in the implant, and the signals command a microprocessor to perform coding tasks. In the current stage, the commands can code for various operations such as performing a designated 0.6 V detection of glucose. This is then issued to a digital to analog converter to form a potential. The measurement task is accomplished by an electrochemical amperometric circuit, voltammetry, one of the electrochemical methods, and a mini-electrode. The internal subsystem, shown in Figure 1(A), is composed of an internal coil, mini-electrode, and the accompanying circuitry.

2.2. Fabrication of mini-electrode

The mini-electrode design, Figure 2(A), consists of a working electrode (WE), reference electrode (RE) and counter (auxiliary) electrode (CE). The electrodes were manufactured according to micro-machining processes (Figure 2(B)).

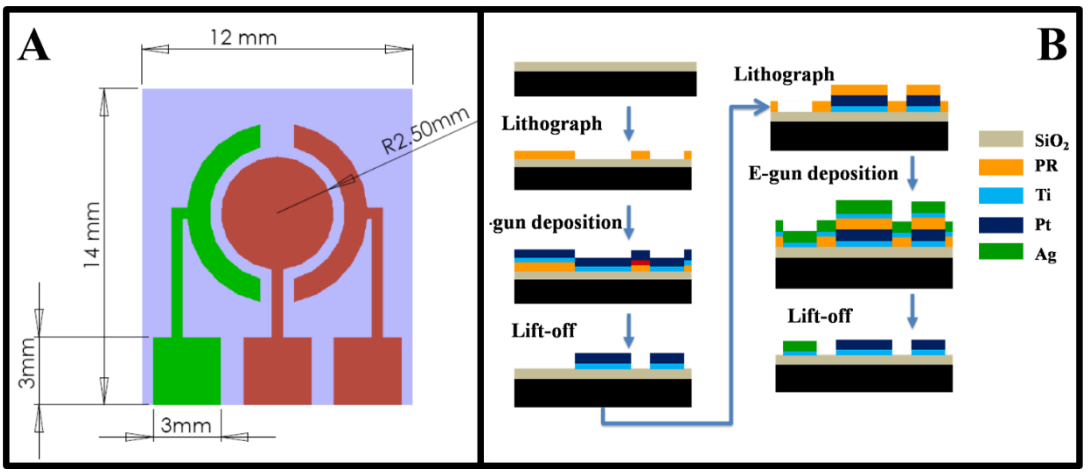

Figure 2. (A) the mini-electrode set design, (B) Micro-machining processes of the fabricated mini-electrode.

Firstly, a silicon substrate is oxidized to form a 100 nm layer of silicon oxide as a barrier. Secondly, lithography is used to deposit a photo-resistance (PR) material as a mask designed with an electrode shape. This step formed the shape of WE and CE, and in the subsequent third step, both of them individually deposited 500 Å of titanium and 1000 Å of platinum. The lift-off process uses acetone as a solvent to dissolve the PR material and remove the unused area around the WE and CE. The silver (Ag) RE was fabricated through the same processes. The RE surface did not form the Ag/AgCl reference electrode. 20 μL of 1 M HCl was dropped onto the surface of the mini-electrode, and utilizing the potentiostatic method applies a 0.7 V between the RE (anode) and the WE (cathode) for 20 sec.

2.3. Preparation of interstitial fluid surrogate

The purpose of implanting biosensors in the subcutaneous tissue of the abdomen is to measure glucose concentration in the interstitial fluid (ISF) [31]. ISF is comprised of proteins, amino acids, fatty acids, sugar, hormones, coenzymes, salts, neurotransmitters, and waste products from cells. When a biomaterial is initially implanted, proteins from the ISF will adsorb and begin foreign body reactions, leading to the fibrous formation. Prior to biosensor implanting, a calibration curve for measuring glucose must be established, however, measuring glucose in phosphate-buffered saline (PBS) is inferior to measuring in ISF conditions. Since it is not practical to collect large quantities of ISF, we produced an ISF surrogate consisting of glucose and various biomolecules. Protein concentration is a key factor in producing a suitable ISF surrogate. A number of studies have reported that protein concentration in ISF ranges between 7 and 34.4 g/L [37-39]. Collison et al use test strips to measure glucose in ISF [40] and ISF surrogates containing diluted plasma from human serum. Protein concentrations in these ISF surrogates range between 11 and 35 g/L.

In this study, we used a diluted serum-based ISF surrogate (Lyphocheck® assayed chemistry control human serum, Level 1, C-310-5), purchased from Bio-Rad, Irvine, CA. As per the specifications of Lyphocheck®, the total protein and glucose concentration were 57.0 ~ 81.9 g/L and 3.87 ~ 6.24 mM, respectively. The serum was diluted 1:2 with 0.1M phosphate buffer solution (pH=7.0) for the ISF surrogate.

Varying amounts of glucose powder were dissolved in the ISF surrogate to create glucose concentrations of 1.67, 6.67, 11.67, 16.67, 21.67, and 26.67 mM. The specification of Lyphocheck® indicated the mean glucose concentration in human serum to be around 5 mM.

2.4. Fabrication optimizing TPU concentration in implantable glucose biosensor

To assess the functionality and accuracy of our sensor, we implanted the unit in rats and continuously monitored the glucose levels. The implant unit with GOx and TPU modification on the electrode set was used for studying the glucose variations in the interstitial tissue fluid of diabetic and normal Wistar rats. In this study, we used rats that weigh approximately 350 grams. Diabetes was induced in rats using Alloxan, a chemical compound that destroys insulin-secreting β cells. Each of these rats received a single dose of 0.525 mL (100 mg/mL, 150 mg/kg Alloxan). Diabetes is typically induced

by day ten. The implant units were subcutaneously implanted in diabetic and control rats on the back near the right thigh. Special care was taken to incorporate the implant unit with the electrode set facing the muscle tissues. It must be noted that prior to implantation, the sensor's glucose calibration curves were obtained using the ISF surrogates and it serves as the standards for subsequent measurements.

In continuously monitored glucose levels study, we compared with ISF and blood glucose levels to validate the results obtained from our device. Figure 3 shows the monitoring equipment to assist us in receiving the signal from the rat. The equipment consists of a cylinder shape animal holder, glucose meter, laptop computer, and our device. To start monitoring the ISF glucose level, the rat was placed into the animal holder. The external coil was placed alongside the holder, near the implantation site (shown in Figure 3). The external controller (subsystem) transmitted a command to trigger the implant subsystem to perform the glucose measurements. The detected glucose signals from ISF buffered for 1 minute. These buffered signals were averaged to output a glucose value, which was then saved and plotted on a laptop computer. Each glucose measurement session lasted for 30 minutes and a time stamp of each was recorded.

To continuously obtain the blood glucose level, an intravenous catheter was pre-inserted into the tail of each rat. An ACCU-CHEK glucose meter was used to read the glucose levels in blood sampled from the catheter and a value was measured every hour. The time stamp was also recorded when the blood was sampled from the rat's tail. When each measurement was complete, the rats were returned to its cage. Both methods were used to continuously monitor glucose levels for 10 hours. After 10 hours period, the data arrays from the two measurement modalities were plotted and the resulting curves provided the time delay for our implanted glucose sensor.

To study the long-term sensitivity of the implanted sensor, we injected 5 mM of glucose each day into the subcutaneous tissue near the implantation site. Upon injection, the system usually responds with a distinct signal, and if the amplitude was lower than the initial measurement, it implied that there was a decrease in sensitivity and stability.

We also used an ACCU-CHEK glucose meter (Roche) to validate the results obtained from our device. The monitoring procedure is as follows:

1. The rat was placed in a cylinder shape animal holder (Figure 3).

2. The external coil was placed alongside the animal holder, near the implantation site. The external controller (subsystem) transmitted a command to trigger the implant subsystem to perform the glucose measurements. The detected glucose signals from ISF buffered for 1 minute.

These buffered signals were averaged to output a glucose value, which was then saved and plotted on a laptop computer. Each glucose measurement session lasted for 30 minutes and a time stamp of each was recorded.

3. An intravenous catheter was pre-inserted into the tail of each rat. An ACCU-CHEK glucose meter was used to read the glucose levels in blood sampled from the catheter and value was measured every hour. The time stamp was also recorded when the blood was sampled from the rat's tail.

4. When each measurement was complete, the rats were returned to its cage. Both methods were used to continuously monitor glucose levels for 10 hours.

5. After 10 hours period, the data array from the two measurement modalities was plotted and the resulting curves provided the time delay for our implanted glucose sensor.

6. To study the long-term sensitivity of the implanted sensor, we injected 5 mM of glucose each day into the subcutaneous tissue near the implantation site. Upon injection, the system usually responds with a distinct signal, and if the amplitude was lower than the initial measurement, it implied that there was a decrease in sensitivity and stability.

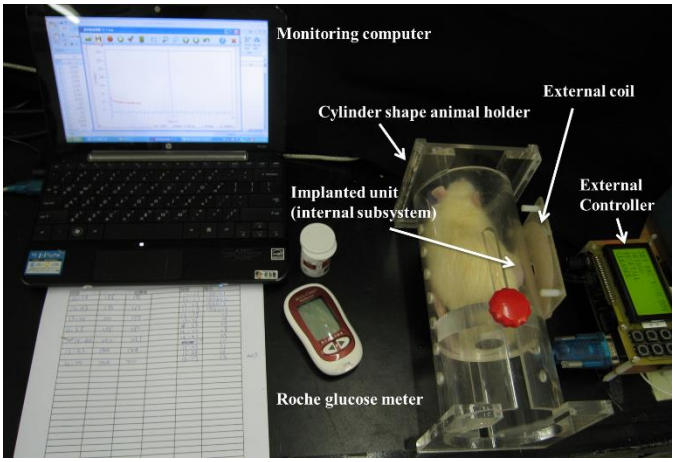

Figure 3. Monitoring equipment including a glucose meter, a cylinder shape animal holder, an external subsystem, and a computer for recording data.

3. RESULTS AND DISCUSSION

3.1. Characteristics of mini-electrode

A commercial platinum electrode (CPE) used in this work and our mini-electrode are different in terms of size and material. Thus, an adjustable function to synchronize the electrochemical performance such as the current responses, potential shift, and ΔEp. of the two electrodes must be achieved. The electrochemical response of the mini-electrode performing its redox reaction operated in PBS and 5 mM ferricyanide. Figure 4 shows the electrochemical features of the commercial electrodes (platinum working electrode, Ag/AgCl reference electrode and platinum counter electrode) and the mini-electrode upon a cyclic voltammogram recorded by AUTOLAB PGSTAT 10 (AUTOLAB). First, the current responses of the CPE were larger than the mini-electrode in both conditions. This signal originated from the reaction area of the working electrode when oxidization or reduction occurred. The CPE area was a diameter 2 mm circle, and the mini-electrode was 2.5 mm.

Second, from Figure 4(A), the reduction peak of the CPE in PBS appeared close to 0.0 V while the mini-electrode recorded a negative potential of -179 mV. To evaluate redox ability, this work used those electrodes to perform the ferri/ferro-cyanide test. The specific ferro/ferri-cyanide has a reversible redox peak, implying that the reduction and oxidation peaks based on the platinum electrode are close to the same potential associated with the value of ΔEp, Therefore, the results in Figure 4(B) indicated the oxidized peaks for CPE and the mini-electrode to be 286 and 178 mV and the reduced peaks to be 175 and 48 mV respectively. A potential shift of the oxidized peak compared to the response of CPE

was 108 mV and was 127 mV in a potential shift of the reduced peak. The potential shifts may have resulted from two major factors; the main one is that an Ag/AgCl reference electrode of the mini-electrode is deficient in saturated potassium chloride. The second is that the platinum material and the counter mini-electrode deposited a thin film of only 100 nm, leading to an imperfect platinum characteristic. Conversely, the CPE is a block of platinum material.

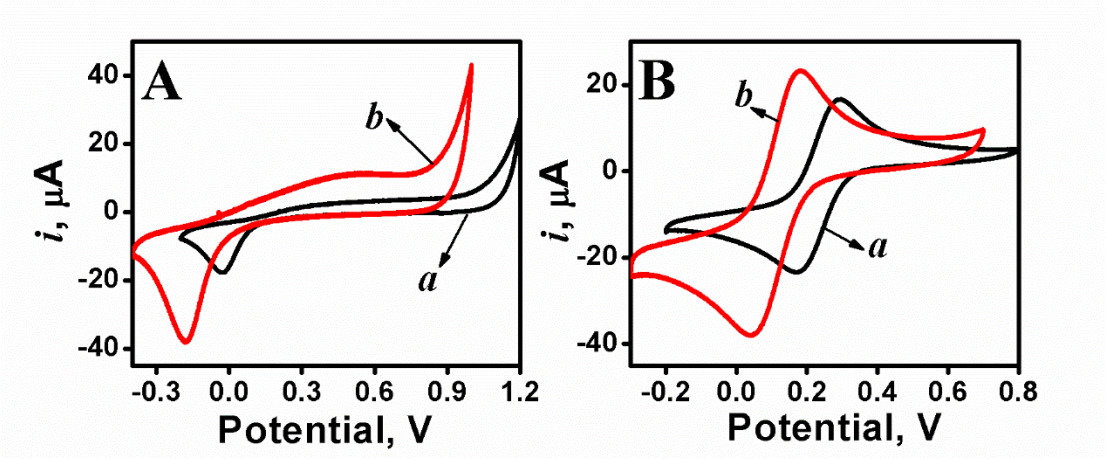

Figure 4. Characteristics of CPE and mini-electrode upon the cyclic voltammetric background (pH 7 phosphate buffer, 0.1 M) responses (A) and the response for 5 mM ferri/ferro-cyanide (B). a and b represent the CPE and mini-electrode independently.

An interesting note about our results is that the ΔEp value, in general, is the differential potential between the oxidation and reduction peak to evaluate redox characteristics. Therefore, it is a reversible species when the ΔEp is close to 0 V oppositely in an irreversible reaction. Given these results, we calculated a difference in the peak potentials between oxidation and reduction in ferri/ferro-cyanide. The results show that the ΔEp of CPE and mini-electrode is 111 mV and 130 mV respectively. Although the ΔEp of CPE is smaller than the mini-electrode, this difference has a slight influence on the electrochemical response. However, to consider the effects of potential shifts and ΔEp, the electrochemical responses still appeared on the mini-electrode. For example, the electrochemical analyzer applies a 286 mV on the CPE (vs. Ag/AgCl) to perform a response of oxidized ferrocyanide, and can also apply a 178 mV for oxidation on the mini-electrode. In other words, the analyzer can provide a suitable potential depending on electrode characteristics for an identical electrochemical reaction/response.

The current work designed a function in which the electrochemical sensor of an internal subsystem can carry out a potential, adjust via a command that the external subsystem transmits, and detect bio-analytes. This adjustable potential function can assist the internal subsystem to perform an identical electrochemical response in comparison to CPE. Therefore, the adjustable function can solve the potential shift so that can perform a successful electrochemical response.

3.2. Performance of the Implantable Glucose Sensing System

The resolution of the implant subsystem was assessed by measuring 10 and 50 M hydrogen peroxide, and its mean net current response was 114 nA (data not shown). This finding implied that a distinguishable current response should be greater than 114 nA.

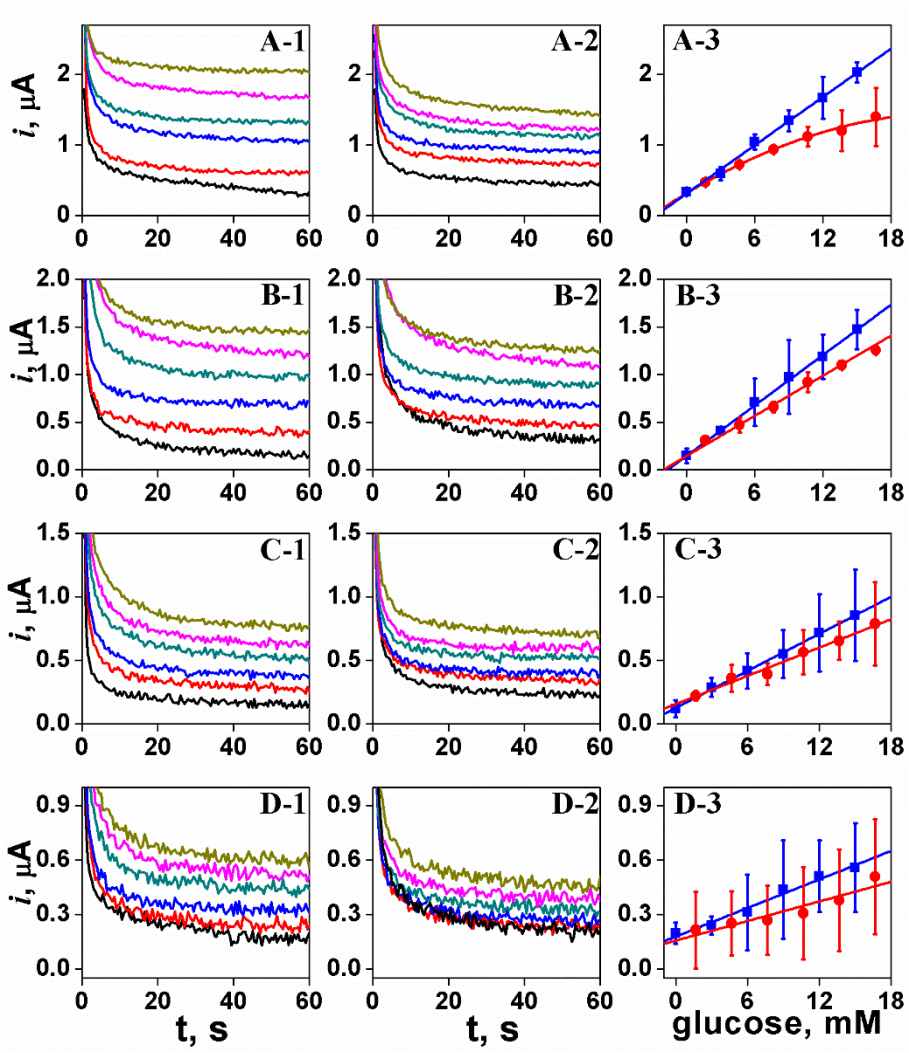

Figure 5. Chronoamperometric curves recorded at 15(A), 20(B), 25(C), and 30(D) mg/mL TPU-based glucose mini-electrode. The test solution was in PBS (-1) and the ISF surrogate (-2). The calibration curves represent (-3), the blue line represents measurement in PBS and the red line represents the ISF surrogate.

Figure 5 shows the chronoamperometry (CA) curves recorded and monitored using a home-made GUI software where the signal fluctuation is manifested. This is possibly contributed from the RF interference in the internal subsystem even though it had anti-EMI tinfoil equipped. Such interference limited the ability of the implantable glucose monitoring system to differentiate changes in glucose concentrations. For the sensing electrode coated with 30 mg/mL TPU membrane, the variation of the signal response (Figure 5(D)) was invisible even upon adding glucose. This was due to the contamination

of RF noise (or interference) whose amplitude overwhelmed the glucose response. The linearity range is another important feature for the biosensor and is generally dependent on analyte reactions to mass transfer control. These characteristics, however, inversely affect the sensitivity of the biosensor. In our sensing electrode configuration, the TPU membrane acts as a mass-transfer barrier by creating diffusion resistance when glucose attempts to penetrate it. Therefore, our enzyme-based must maintain appropriate balance between linearity and sensitivity to assure perceivable signal responses. The electrode sensitivity for various TPU membranes applied. The sensitivity decreased with the increase of the TPU concentration, implying that mass transfer controlled the electrochemical behavior. The AUTOLAB recordings indicated that the 30 mg/mL TPU-modified mini-electrode showed an excellent performance in reducing protein adsorption (data not shown). In addition, the results also suggested that the calibration curves for sensing glucose both in PBS and in ISF surrogate nearly overlapped. Due to the RF interference, however, the electrode used for in vivo tests required a TPU membrane of 20 mg/mL rather than 30 mg/mL. This resulted in increased pore size and glucose penetration. As a result, the glucose signal response becomes more distinct.

3.3. Continuous Monitoring of Glucose Levels

To continuously monitor glucose levels, the internal subsystem was implanted in the subcutaneous tissue of normal and diabetic rats. The incision site for all the rats was near the leg, on the gluteus superficialis, between the lumbodorsal fascia and biceps femoris. After insertion of the internal subsystem, the incision was stitched up with surgical silk. Special care was taken to avoid the wound inflammation. Figure 6 shows the glucose levels of two normal rats measured from the ISF and blood. Monitoring began when the rats were first observed eating food because the blood sugar levels were expected a rise. In the first normal rat, the Roche glucose meter revealed two major glucose surges at 16:06 and 18:11 (Figure 6(A)). Corresponding blood sugar responses were detected by our system and appeared at 18:58 and 21:00. Each peak had a delay of about 170 minutes. After it was sacrificed, the internal subsystem and implantation site were examined for adipose tissue morphology. The dense tissue may have created a diffusion barrier when glucose was transported from blood vessels to the ISF. In the second rat, however, the ISF signal response by our system exhibited a lag time of about 30 minutes (Figure 6(B)). In addition, there was no adipose tissue surrounding the implantation position in the second rat. According to a related research report [41-43], this lag time is associated with the size of the implanted device, local tissue interaction, intrinsic sensitivity, glucose diffusion from vessel to ISF.

The glucose levels in diabetic rats revealed significant changes after eating and insulin injections (Figure 6(C)). After the first diabetic rat had food, it was subsequently placed in a cylinder-shape animal holder (Figure 3) for the study. Figure 6(C) shows the blood glucose level variation (triangle) in four time periods as recorded by the Roche glucose meter. The first period shows an increase from 442 to over 600 mg/dl glucose between 13:05 and 14:05. The Roche glucose meter used in this study is limited in the range between 10 and 600 mg/dl. Whenever the blood glucose level exceeds 600 mg/dl, the meter shows a symbol of “H1” to indicate that the value is over its detection range. Therefore, when the meter displayed “H1”, we recorded the blood glucose level as 600 mg/dl. In the first period, the signal response

from ISF increased as measured by our glucose monitoring system. It took one hour to arrive in a steady state. As mentioned above, the lag time depends on the device size, the local tissue interaction, and mass transfer/diffusion. In the second period, the glucose levels reached a steady state between 14:05 and 18:01. This is possibly a result of the destruction of pancreatic β-cells in the diabetic rat by Alloxan and thus were unable to secrete insulin for glucose metabolism. The blood glucose levels remained high until a 10 unit insulin injection was given. Furthermore, our glucose monitoring system indicated that the signal response from the ISF reached a steady state between 15:07 and 19:30, showing a 60-minute lag time. In the third period, insulin was injected at 18:01 and the Roche meter's recording of the blood glucose level decreased from 565.5 to 135 mg/dl in about 60 minutes. The time of the glucose level lowering down was approximate at 18:40. On the other hand, the declining signal response of ISF detected by our system started around 19:30, which indicates a 50-minute delay. In the final period, the blood glucose remained at normal levels, pointing to a successful reaction to insulin treatment.

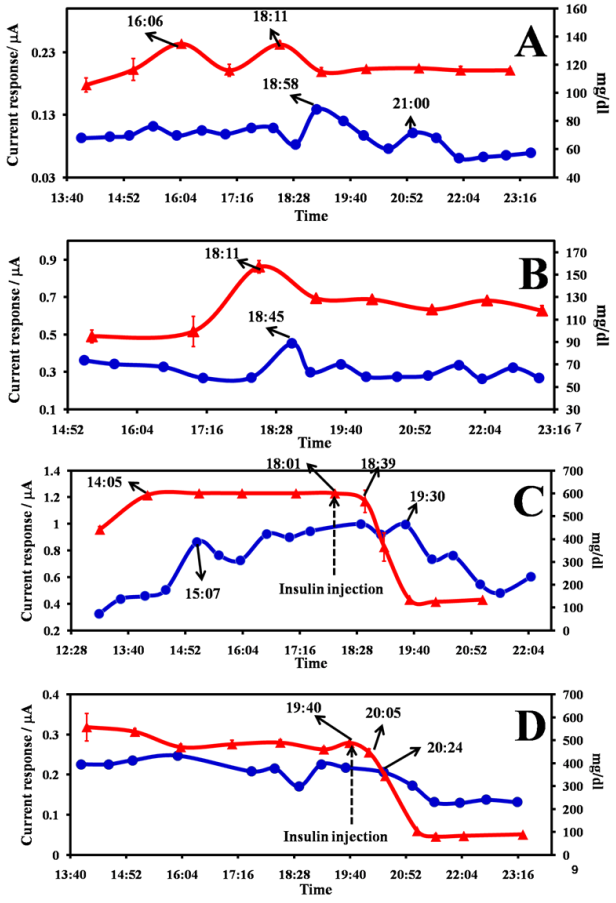

Figure 6. Glucose level variation study in normal rats recorded by a glucose meter (triangle) and the developed system (circle). The unit of blood glucose levels is mg/dl. The unit of the current response for ISF detected by the system is A. (A, B) represents the first and the second normal rats, (C, D) the first and the second diabetic rats.

Figure 6(D) shows that the second diabetic rat had a glucose surge between 14:02 and 19:40 as recorded by both the glucose meter and our implanted sensor. At 20:05, a 10-unit insulin injection was

given and one hour later, both sensors revealed a significant decrease in glucose levels from 447 to 104 mg/dl.

Rebrin performed a similar study but instead used a needle type of glucose sensor and reported a 10-minute lag time [41]. Based on their study, they established a glucose diffusion model from vessels to muscle tissues. Furthermore, they concluded that the lag time has something to do with the size of the implanted device, local tissue interaction, intrinsic sensitivity, glucose mass transfer/diffusion (from vessel to ISF). Since they took into account the size of the implanted device, the needle biosensor was applied. The initial testing of our glucose sensor showed that the detection lag time in both normal and diabetic rats is very large. One likely cause is that due to the size of the internal subsystem, it created was a barrier that prohibited glucose diffusion from blood vessels to the muscle.

3.4. Stability of the Implantable Glucose Sensing System

The stability of an implantable glucose biosensor is an important factor if the device is expected to be used long term. Therefore, this work presents a method to study the stability issue. Each day, 5 mM of glucose was injected in the area surrounding the implantation position. During daily injections of a fixed dose of glucose in rats, the implanted electrode recorded an attenuated signal response each time (Figure 7).

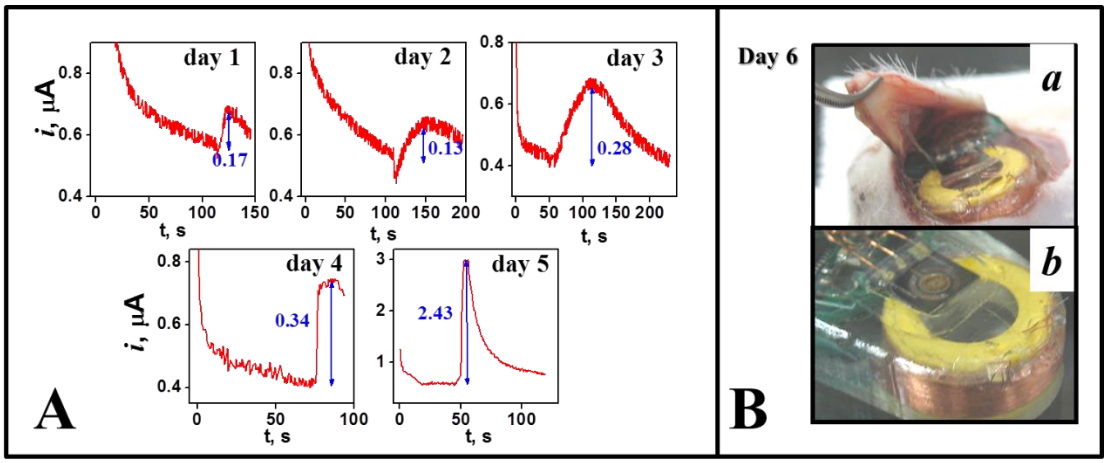

Figure 7. The response of the sensing system was a current/time course study. In day 6, the pictures show the adherence between the life-off membrane and the onsite dermis. (A) The stability study by monitoring the time course of the developed wireless implantable sensing system's responses (upon injection of 5 mM glucose). (B) (a) The lift-off TPU membrane adhered to the dermis; (b) The internal subsystem damaged by the rat.

Compared to the initial measurement, there was a 23 % reduction in signal amplitude 2 days after the implantation. This was due to tissue and immune response which was triggered by foreign objects. The surface of the implanted sensor adsorbed proteins, forming a fibrous encapsulation barrier that obstructed glucose diffusion. However, in vitro tests with ISF surrogates revealed that the TPU

membranes were able to resist protein adsorption. Unfortunately, implanting the internal subsystem in the subcutaneous tissue of rats created issues such as inflammation, membrane biofouling, fibrous encapsulation, and loss of enzyme activity. Interestingly, on the third day, the signal response increased significantly and was even larger than that measured on the first day. At the 5th day, the glucose signal response was dramatically enlarged. The cause was that the TPU membrane was adhered to the dermis and then peeled off when the rat moved around (Figure 7(B)). It is known that wound healing involves four sequential phases: hemostasis, inflammatory, proliferative and remodeling [44-46]. During the proliferative and remodeling phases, in particular, the stitched incision sites become itchy. As a result, the rat bit off the surgical silks which lead to wound rupture at the 6th day. When the rat was sacrificed, it was revealed that the coil of the internal subsystem was broken and lost its functionality (Figure 7(B)).

4. CONCLUSIONS

In this study, we developed an implantable glucose sensor and tested its functionality in rats. By continuously monitoring the glucose signal, we are able to evaluate the stability of the system and its interaction with a semi-permeable membrane (TPU).

The detection of biomarkers such as glucose is based on specific enzyme immobilization. We are able to immobilize enzyme and mediator using TPU. TPU performed quite well in terms of protein adhesion resistance. Careful preparation of the TPU concentration is essential as the membrane pore sizes could alter the signal response of the biosensor dramatically. Our study showed that 20 mg/mL was an adequate concentration to be used in our RF-based implantable glucose monitoring system is. Although the electrode prepared with such a concentration compromised the sensitivity of the system, it tolerated the RF interference reasonably well.

In addition to the studies on semi-permeable membranes, this dissertation created an implantable glucose monitoring system, which involves the significant effort of system integration. This work included the development of an external controller (subsystem) and an implantable unit (subsystem). The external controller serves as a human-system interaction interface as well as the electric power driving force for the implant unit. It is important to note that the aforementioned Class E power amplifier is the key design in the wireless communication scheme. The amplifier not only converts direct current to alternate current but also effectively enlarges the amplitude of the current. The integration of the implant unit is one of the core parts of this work, which consisted of the mini-electrode implementation, the bi-directional wireless transmission electrochemical sensor implementation, and its assembly. The mini-electrode implementation includes GOx immobilization and TPU membrane coating on the electrode. The bi-directional wireless transmission electrochemical sensor implementation was composed of the assembly and sealing of the antenna coil, the RF circuitry, and the sensing circuitry. The functionality of the glucose monitoring system was confirmed by using in vitro test to measure glucose concentration in ISF.

The developed implantable glucose sensing system was used in in vivo studies. The implant unit with GOx and TPU membrane modified on the electrode set was used in studying glucose variations in ISF of diabetes-induced and normal Wistar rats. Results show that the intravenous and ISF glucose levels

revealed a 30 to 170 minutes delay. We believed that it is due to the size of the internal subsystem, which acted as a barrier, prohibiting the glucose diffusing from vessels to the muscle tissues. Another possible explanation for the time lag is due to biofouling caused by excessive protein adhesion. After the rat was sacrificed, there was evidence for fibrosis around the internal unit. Although the biomarker presented in this work was glucose, the developed wireless implantable sensing system is able to detect other biomarkers such as our working on-progress projects on uric acid, cholesterol, and dopamine with a minor work of substituting corresponding enzymes. We find that the wireless sensing system is a superior platform to conduct in-vitro and in-vivo studies.

ACKNOWLEDGEMENTS
This work was supported by the Zhaoqing city of Guangdong province Science and Technology Innovation Strategy Special Fund (No. 2018N005).

References

1. D. Q. Jian, M. Z Wen, D. Jin, W. Rui, P. L. Ru, *Anal.Biochem.,* 385 (2009) 264.
2. T. Hao, H. C. Jin, Z. Y. Shou, H. N. Li, H. D. Guo, F. K. Ya, *Anal.Biochem.,* 331 (2004) 89.
3. W. B. Paul, S. P. Robert, S. S. Michael, *Anal.Chem.,* 77 (2005) 7556.
4. D. W. Xu, X. D. Hai, Y., Z. Ting, J. L. Zhi, B. Z. Jing, X. X. Zhao, C. Xi, Y. W. Kwok, N. C. Guo, R. W. Xiao, *Biosens.Bioelectron* 24 (2009) 3702.
5. P. Hyunggoo, S. Y. Hyung, P. Umakant, A. Rani, L. Juho, L. Juhwan, L. Woonhyoung, C. J. Seong, *Biosensors and Bioelectronics* 54 (2014) 141.
6. J. T. La Belle, A. Adams, C. E. Lin, E. Engelschall, B. Pratt, and C. B. Cook, *Chem. Commun.*, 52 (2016) 9197.
7. Y. Z. Zhu, X. U. Meng, Y. Q. Chen, J. Li, H. Y. Shao, Y. Lu, L. B. Pan, Y. C. Xu, and J. Cheng, *Sensor. Actuat. B-Chem.*, 303 (2020) 127235.
8. G. S. Wilson, and Y. Hu, *Chem. Rev*., 100 (2000) 2693.
9. J. Wang, *Chem. Rev*., 108 (2008) 814.
10. T. Xiao, F. Wu, J. Hao, M. Zhang, P. Yu, and L. Mao, *Anal. Chem*., 89 (2017) 300.
11. H. A. Syed, and G. Saira, *Diabetes Ther*., 11 (2020) 2453.
12. H. Blauw, A. J. Onvlee, M. Klaassen, A. C. van Bon, and J. H. DeVries, *Diabetes Care*, 44 (2021) 836.
13. W. K. Ward, L. B. Jansen, E. Anderson, G. Reach, J. C. Klein, and G. S. Wilson, *Biosens. Bioelectron.*, 17 (2002) 181.
14. B. Yu, L. West, Y. Moussy, and F. Moussy, *IEEE Sens. J*., 8 (2008) 97.
15. F. Wu, P. Yu, and L. Mao,. *Curr. Opini. Electroche.*, 5 (2017) 152.
16. N. O. Sokal, and A. D. Sokal, *IEEE J. Solid-St. Circ*., 10 (1975) 168.
17. J. Ebert, M. Kazimierczuk, *IEEE J. Solid-St. Circ*., 16 (1981) 62.
18. G. Andrei, and H. R. Frederick, *IEEE Microw. Mag*., 19 (2018) 26.
19. M. Hayati, S. Roshani, S. Roshani, M. K. Kazimierczuk, and H. Sekiya, *IEEE T. Power Electr.*, 33 (2018) 2571.
20. K. Surakitbovorn, and J. M. Rivas-Davila, *IEEE J. Em. Sel. Top*. P., 99 (2020) 1.
21. P. R. Troyk, and M. A. K. Schwan, *IEEE T. Bio-med. Eng*., 39(1992) 589.
22. H. Naderi, M. M. Matin, and A. R. Bahrami, *J. Biomater. Appl*., 26 (2011) 383.
23. R. R. Costa, and J. F. Mano, *Chem. Soc. Rev.*, 43(2014) 3453.
24. J. Xu, and H. Lee, *Chemosensors*, 8(2020) 66.

25. S. Bian, B. Zhu, G. G. Rong, and M. Sawan, *J Pharm. Anal*., 11 (2021) 1.
26. R. T. Tran, J. Yang, and G. A. Ameer, *Annu. Rev*., 45 (2015) 277.
27. L. Zhou, H. Hou, H. Wei, L. Yao, L. Sun, P. Yu, B. Su, and L. Mao, *Anal. Chem*., 91 (2019) 3645.
28. D. Rodrigues, A. I. Barbosa, R. Rebelo, I. K. Kwon, R. L. Reis, V. M. Correlo *Biosensors*, 10 (2020) 79.
29. Z. X. Deng, J. W. Tao, L. J. Zhao, W. Zhang, Y. B. Wang, H. J. Mu, X. X. Xu, and W. Zheng, *Process Biochem*., 96 (2020) 73.
30. Y. Noguchi, Y. Iwasaki, M. Ueda, and S. Kakinoki, *J. Mater. Chem.* B, 8 (2020) 2233.
31. J. O. Jeong, S. Kim, J. Park, S. Lee, J. S. Park, Y. M. Lim, and J. Y. Lee, *J. Mater. Chem*. B, 8 (2020) 7225.
32. S. Mross, T. Zimmermann, N. Winkin, M. Kraft, and H. Vogt, *Sensor. Actuat. B-Chem.*, 236 (2016) 937.
33. M. Avula, D. Jones, A. N. Rao, D. McClain, L. D. McGill, D. W. Grainger, and F. Solzbacher, *Biosens. Bioelectron*., 77 (2016) 149.
34. Y. Ahmadi, and K. H. Kim, *TrAC Trend. Anal. Chem*., 126 (2020) 115881.
35. H. F. Wang, X. Liu, D. E. Christiansen, S. Fattahpour, K. Wang, H. Q. Song, S. Mehraeen, and G. Cheng, *Biomater. Sci*., 9 (2021) 1381.
36. G. S. Wilson, and M. A. Johnson, *Chem. Rev*., 108 (2008) 2462.
37. K. Aukland, and H. O. Fadnes, *Acta. Physiol. Scand*., 88 (1973) 350.
38. L. S. Petersen, J. K. Kristensen, and J. Bülow, *J. Invest. Dermatol*. 99 (1992) 357.
39. N. F. Andersen, B. M. Altura, B. T. Altura, and A. O. Siggaard, *Clin. Chem*., 41 (1995) 1522.
40. M. E. Collison, P. J. Stout, T. S. Glushko, K. N. Pokela, D. J. Mullins-Hirte, J. R. Racchini, M. A. Walter, S. P. Mecca, J. Rundquist, J. J. Allen, M. E. Hilgers, and T. B. Hoegh, *Clin. Chem*., 45 (1999) 1665.
41. K. Rebrin, G. M. Steil, W. P. van Antwerp, and J. J. Mastrototaro, *Am. J. Physiol. Endoc. M*, 277 (1999) E561.
42. C. Chen, X. L Zhao, Z. H. Li, Z. G Zhu, S. H Qian, A. J. Flewitt, *Sensors*, 17 (2017) 182.
43. J. Xu, H. Lee, *Chemosensors*, 8 (2020) 66.
44. J. V. Quinn, M. D. Philadelphia, and B. C. Decker, *Acad. Emerg. Med*., 6 (1998) 869.
45. M. H. Periayah, A. S. Halim, A. Z. M. Saad, *Int J Hematol Oncol Stem Cell Res.*, 11(2017) 319.
46. S. Ellis, E. J. Lin, D. Tartar, *Current Dermatology Reports*, 7 (2018) 350.